Effective Multitier Network Model for MRI Brain Disease Prediction using Learning Approaches

N.Ravinder[1]
Research Scholar
Department of CSE, Koneru Lakshmaiah Education Foundation, Vaddeswaram, AP, India

Dr. Moulana Mohammed[2]
Professor
Department of CSE, Koneru Lakshmaiah Education Foundation, Vaddeswaram, AP, India

***Abstract*—Brain disease prognosis is considered a hot research topic where the researchers intend to predict the clinical measures of individuals using MRI data to evaluate the pathological stage and identifies the progression of the disease. With the lack of incomplete clinical scores, various existing learning-based approaches simply eradicate the score without ground truth score computation. It helps restrict the training data samples with robust and reliable models during the learning process. The major disadvantage of the prior approaches is the adoption of hand-crafted features, as these features are not well-suited for the prediction process. This research concentrates on modelling a weakly supervised multi-tier dense neural network model ($ws-MTDNN$) for examining the progression of brain disease using the available MRI data. The model helps analyze the incomplete clinical scores. The preliminary ties of the network model initially haul out the distinctive patches from the MRI to extract the global and local structural features (information) and develop a superior multi-tier dense neural network model for task-based image feature extraction and perform prediction in the successive tiers for computing the clinical measures. The loss function is adopted while examining the available individuals even in the absence of ground-truth values. The experimentation is done with the available online Dataset like ADNI-1/2, and the model works effectually with this Dataset compared to other approaches.**

Keywords*—Brain disease; learning approaches; ground truth value; feature learning; global and local feature analysis

I. INTRODUCTION

Magnetic resonance imaging (MRI) is a suitable imaging technique for the head (specifically the brain) used in everyday clinical practice. It enables doctors to assess the nervous system's health and identify the existence of specific disorders. The computer-aided Alzheimer's disease (AD) prediction and premonitory phase, moderate cognitive decline (MCI), has made extensive use of MRI in recent years [1]–[6]. Anatomical MRI may detect aberrant brain structure and find imaging biomarkers for Alzheimer's disease (AD) in medical settings without radiation or other invasive procedures. Lately, assessing the state of disease and forecasting outcomes of AD and MCI progress employing baseline (BL) MRI information has been a popular issue.

Although numerous machine-learning approaches have already been developed for risk ratings utilizing BL MRI [11], a frequent difficulty of current systems is inadequately labelled information; participants may ignore ground-truth diagnostic marks at specific time, amongst 805 participants inside AD Neural correlates Initiative-1 (ADNI-1) database [7]-[10], only 622 & 631 individuals had full CDR-SB & MMSE ratings 24 months following BL time, correspondingly. Earlier research simply discarded patients with incomplete clinical ratings owing to the sensitivity of reinforcement methods. Coupe [11] evaluated improvements of two clinical indicators from MRI utilizing 186 participants with comprehensive ground-truth clinical ratings from ADNI-1. Removing individuals with incomplete scores reduces the training dataset, decreasing the efficiency and resilience of estimation techniques. Furthermore, earlier machine-learning approaches often fed predetermined interpretations [e.g., image strength and tissue volume inside regions-of-interest] to ensuing prediction models, even though these characteristics may not be optimum for estimation techniques decreasing prognosis effectiveness.

The performance of deep learning methods has inspired various researches to use convolutional neural networks (CNN) to identify MRI characteristics for identifying certain diseases. Moreover, these techniques often fall inside the supervised learning method, making it impossible to train networks using people whose diagnostic ground-truth scores aren't full. Using all relevant poorly classified models (training participants with inadequate ground-truth scores at key time-points) is critical in Magnetic resonance brain illness diagnosis.

This research proposes the weakly supervised deep neural network ($ws-MTDNN$) for cerebral illness prediction utilizing BL MRI and partial clinical ratings at several time points. We define the following MR images and then identify multi-resolution image patchwork which relies on AD-based features. Finally, the deep CNN for forecasting of different clinical ratings at several points in time is created. This CNN has a novel weighting nonlinear function that enables the systems to learn sparsely labelled training data. Unlike prior MRI-based investigations, our suggested $was-MTDNN$ technique can train models using all accessible individuals, even if some lack medical ratings at key periods[12][13]. Also, our anatomy landmark-based multi-resolution patch extraction procedure may address the issue of limited data by employing texture features instead of whole 3-D MR images as training examples.

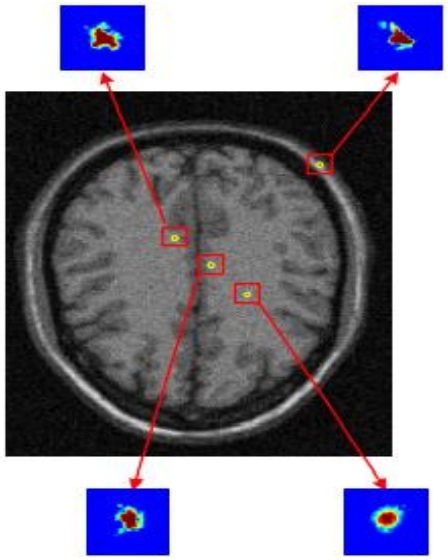

Fig. 1. Input MRI Image.

This section is used to summarise the paper's key contributions. First, unlike earlier researches [11], [17], we create a computational model with such a balanced gradient descent that can use all accessible weakly labelled patients (i.e., with partial ground-truth clinical ratings). It allows us to use all accessible labelled subjects. Integrating additional individuals in the training phase might aid in strengthening the resilience of the learnt system. Secondly, we suggest extracting variations in terms (as opposed to fixed-sized) input images if both small & large-scale patches centred at every location are retrieved. Our process is based on anatomic structures relevant to AD. This kind of approach assists in capturing the local/global analytical brain information [16]. Third, we create a combined prediction technique that simultaneously estimates many clinical scores at various times. The collaborative learning technique is anticipated to mimic the natural link between scores at/across various time points, aiding in the improvement of predictive performance. Using an MR image of a fresh experiment, the suggested technique can estimate four clinical ratings at four time-points in 12s, which is near to instant response. The research contributions are:

1) The input image is pre-processed for noise removal with Weiner filter and the contrast histogram equalization (CLAHE) is used for pixel block selection.

2) The weakly supervised multi-tier dense neural network model ($ws - MTDNN$) is proposed to perform the classification process.

3) The performance is evaluated with indices like accuracy, specificity, sensitivity and error rate.

The work is provided as: Section II provides the comprehensive analysis of various prevailing approaches; Section III gives methodological analysis using pre-processing and IV is methodology explanation. The outcomes are discussed in Section 5 and summary in Section VI.

II. Related Work

In this part, we first discuss the standard interpretations of central nervous system MRIs before showcasing current MRI-based machine learning research to forecast and detect brain diseases. Many different features extracted from brain MRI have indeed been created in the research for automated AD/MCI prediction and diagnosis. These models may be loosely divided into three phases: voxel information, ROI recognition and patch recognition. More information on each type is provided as follows.

Voxel techniques [18] evaluate brain MRI by accurately measuring local tissues density (white and grey matter) following rigid normalization of actual brain images [19]-[20]. Sherubha et al. [21] suggested identifying volumetric information from specific brain parts from MR scans and then using them to categorize gender and AD. Moreover, voxel approaches are generally premised on the 1-1 anatomy mappings among participants and Gaussian dispersion of focal organ concentrations throughout statistical testing [23]. To suit the voxel description, tissue density is distorted with larger cones at the price of focused precision, which may lessen the voxel-based representation's racist and discriminatory potential for MRIs. Some downside of voxel-based modelling shows the amount of training data for individuals is typically quite small, resulting in the small-sample-size issue [24] and decreasing the effectiveness of learnt models. ROI-based depictions concentrate on assessing locally anatomical quantities in the mind's designated areas, in contrast to voxel-based characteristics. In example, earlier ROI-based studies often use tissue volume [11], [25]-[27], cortical thickness [28], hippocampal volume, and tissue densities in specific areas of the brain as feature extraction of MR data. This sort of representation, however, calls for an a priori hypothesis about aberrant areas from a structural standpoint to designate sections, even though these notions may not hold in actuality [22]. A defective brain area may cover numerous ROIs or only a tiny section of an ROI; therefore, employing a fixed brain division may reduce learning performance.

Patch-based analysis three was created to identify minute anatomical differences in brain MRIs using nonlinear analyses to represent the one-to-many mappings between brain structures. According to the author, the patch-based analysis may help diagnose AD and evaluate MCI development. Mohan et al. [28] used GM concentration within image regions as MRI for Disease prediction. The author suggested extracting morphometric information (local energy distribution) using AD-related anatomic structures. These carefully created MRI characteristics are often used to feed established models (such as SVMs and model structure [28]) for the diagnosis and prediction of diseases. However, given that the process of image retrieval and machine learning are carried out separately in these approaches, the pre-extracted MRI features in question may not be the most effective estimation techniques. Numerous supervised learning approaches have been developed to learn MRI characteristics that are task-oriented [14] [15]. An MR scan has millions of vertices, so many brain areas may not have been impacted by Alzheimer's. As a result, one of the main challenges in MRI-

based transfer learning is figuring out how to identify correctly (e.g., discriminatively across groups) in MRIs.

To overcome this trouble, Myronenko et al. [29] suggested concentrating on three ROIs (i.e., the hippocampus, ventricle, and neuroimaging surface) and created the deep CNN for risk that exists in measurements of participants using 2D texture features taken from the three ROIs. In brain scans (i.e., architectural MRI and mobility tensor image information), the CNN used the hippocampus ROI and adjacent areas. Similarly, the author published a deep ranking algorithm for classifying AD from the hippocampus ROI. These studies employ experimentally identified MRI areas without addressing other possibly essential brain regions. The author created a 2D CNN to distinguish AD patients using functional and structural MRI scans. However, they reduce 3D and 4D images to 2D slices and give inputs to the networks, neglecting the crucial spatial information. Recently, Risk et al. [30] developed an anatomic heritage site deep learning system for Clinical examination and MCI conversion prediction. To be more precise, they first identify 3-D image patches using brain regions with AD-related anatomic structures, and afterwards, they create a CNN for combined MRI extracting the features and disease categorization. However, set the size of texture features is employed in these investigations, disregarding the possibility that structural alterations brought on by dementia might differ significantly across various brain areas.

Additionally, most current deep learning techniques are completely regulated, with individuals lacking ground-truth ratings at certain intervals simply being eliminated. To properly engage all available patients (including those lacking ground-truth ratings) for training, a semi-supervised CNN is presented for prediction of MRI data. The suggested approach departs from the earlier research in [30]. In this research, we employ weakly labelled training items by designing a distinctive weighted nonlinear function in the suggested neural net, while earlier techniques [30] can only use completely labelled (whole ground-truth score) training cases. This article attempts to extract multi-resolution input images centred at each landmark site to simulate brain MRI multi-resolution spatial features, whereas only uses fixed-sized input images.

III. Data Acquisition

We conducted trials on 1469 individuals drawn from subsets of the accessible Dataset collected [10], namely ADNI-1/2. 805 participants have BL structured MRI data from ADNI-1, and 664 individuals from ADNI-2. Individuals are immediately deleted from ADNI-2 if they feature for both ADNI-1 and ADNI-2. In contrast to the participants in ADNI-1, who had 1.5 T T1-weighted MRI, ADNI-2 had 3.0 T T1-weighted MRI. In our investigations, ADNI-1/2 are two separate databases. These issues may be divided into three groups based on several criteria: AD, MCI, and HC.

Four clinical criteria are utilzied: 1) CDR-SB; 2) ADAS-Cog11, a different form of the ADAS-Cog with 11 items; 3) ADAS-Cog13, a 13-item version of the ADAS-Cog; and 4) MMSE. The BL time following approval is the day individuals were supposed to conduct the screening. Additionally, the length beginning from the BL time indicates the time points for obeying visits. Every participant under investigation has MRI data at baseline. However, many lack ground truth scores for certain clinical parameters at particular periods. Table I displays comprehensive details on the topics under study. For each subject's structural MR imaging, we first correct the anterior-posterior commissures, strip the skull and remove the cerebellar. Next, we align every image to a shared Colin27 template before resampling all MR images with a horizontal spatial resolution. Finally, we adjust brightness heterogeneities for each MR image using the N3 method.

A. Weiner Filter

It provides a substantial role in various applications like echo cancellation, linear prediction, signal restoration, system prediction and channel equalization. The Weiner coefficients are evaluated to reduce the average squared distance among the desired input and the filtered output. The proposed filter theory considers the inputs that are stationary process. When the filtering coefficients are re-evaluated at periodic intervals for every blocks of 'N' signal samples then the filter needs to adapt the average signal characteristics within the block and works block adaptively. It is determined to be stationary over the relatively small sample blocks. The target of Weiner filter is reducing the mean square error value and image restoration. It is expressed as in Eq. (1):

$$x(n) = d(n) + v(n) \tag{1}$$

Here, $d(n)$ and $v(n)$ represents stationary random process.

B. Contrast Limited Adaptive Histogram Equalization

The following are the CLAHE procedure:

1) Partition the image into number of equal sub-blocks (size) and every sub-block should be non-overlapping and continuous.

2) Measure the local histogram of every sub-block;

3) Evaluate the average number of pixels allocated to sub-block gray level ($Avnum$). When $GrayNum$ is utilized to specify the probable gray level to sub-blocks, the process is depicted in Eq. (2) where XP and YP represents the number of pixels in $X\ and\ Y$ sub-block directions.

$$AvNum = \frac{XP.YP}{GrayNum} \tag{2}$$

4) The shear coefficient CV is fixed with a range of [0,1]. For various images, it can be adjusted to provide superior value via the simulation outcomes, and the actual shear limit value NV is expressed as in Eq. (3). Here, round specifies the rounding off function.

$$NV = Avnum + round\ (CV.(XP.YP - AvNum) \tag{3}$$

5) With the shear limit, the pixels for every gray level of local histogram and the added number of pixels are re-distributed to every gray level of histogram. Consider, that $Nclip$ specifies the total amount of pixels that are eliminated. Therefore, the number of pixels can be attained NA_{cp} that every gray level is allocated with Eq. (4) and Eq. (5):

$$Nclip = \sum(\max(H(i) - NV, 0)) \quad (4)$$

$$NA_{cp} = \frac{NClip}{GrayNum} \quad (5)$$

Here, CH is the histogram after the re-distribution process and it is attained by Eq. (6):

$$CH(i) = \begin{cases} NV & H(i) > NV \\ NV & H(i) + NA_{cp} \geq NV \\ H(i) + NA_{cp} & else \end{cases} \quad (6)$$

6) Consider that the remaining amount of pixels after distribution is $NumLeft$, step distribution size is depicted as:

$$Step = \frac{GrayNum}{Numleft} \quad (7)$$

Initiate searching from minimal gray level by step size; therefore the pixels are allocated when the numbers of pixels are lesser than shear threshold. Then, finish the cycle from the minimal to maximal gray level till $Numleft$ is set to zero. Therefore, the histogram allocated is fulfilled and some new histogram is acquired.

7) Histogram equalization is done on every sub-region after the shearing process.

8) The centre-point sub-blocks is considered after the reference point acquired form the gray value. Every image pixel is executed by bilinear interpolation and pixel mapping is provided using the related regions with adjacent reference points. Assume, the small rectangle (x, y) specifies target point and $f(x, y)$ represents gray value to evaluate (x, y). The adjacent regions' center point is provided as $A(x-, y-), B(x+, y-), C(c-, y+) and\ D(x+, y+)$. The gray level value $f(x, y)$ is specified as linear gray value combination with four points. For every pixel over the boundary regions, gray level is evaluated using the linear interpolation adjacent sample points where the corner points are evaluated with the adjacent sample points as in Eq. (8):

$$f(x, y) = a[bf(x-, y-) + (1 - b)f(x+, y-)] + (1 - a)[bf(x-, y+) + (1 - b)f(x+, y+)] \quad (8)$$

$$a = \frac{y-(y-)}{(y+)-(y-)} \quad (9)$$

$$b = \frac{x-(x-)}{(x+)-(x-)} \quad (10)$$

IV. Methodology

In this study, we aim to address two difficult issues in MRI-based brain illness prediction: how to fully exploit poorly labelled training data (i.e., individuals with inadequate ground-truth medical ratings) and how to learn important characteristics of MR images structurally. A weakly supervised CNN is created to incorporate extraction of features and model learning into a cohesive framework, using all accessible weakly labelled subjects for the training phase. The suggested $ws - MTDNN$ approach consists of two basic steps: extracting multi-scale image patches and classification. More information is provided below. There are thousands of voxels for each brain MR imaging, yet dementia's structural alterations may be minor. When the complete MR image is provided to the deep learning model, the inputs contain much loud noise data, making network development challenging with just a few hundred training subjects. To train the classifier for accurate illness prediction, we want to find important brain areas in each MRI rather than utilizing the complete image.

We use anatomical markers to find AD-related areas. Here, landmark detection is used to derive 1741 anatomical structures from the Colin27 templates. Numerous landmarks are geographically adjacent to one another, as can be seen in the supplemental materials in Fig. 2. To avoid data duplication and computation time, we chose K = 40 anatomical landmarks. We initially sorted those features in order of increase using the p-values that the landmark identification method obtained via a correlation among AD and HC individuals. The spatial Distance measure is provided to limit (i.e., 20) the separation among landmarks, and we use the top K = 40 monuments. For example, we display the recognized features on three individuals and these landmarks in the templates region.

We generate multi-resolution texture features from an input MRI using these landmarks to obtain extra depth information. Specifically, we derive both small and large scale regions out of MRI. Those patches are all centred on the respective landmarks. So, provide *K* landmarks, we can get 2K image patches of certain MRI. These multi-resolution image patching serve as the input information for suggested model.

We simultaneously conduct pattern recognition of MRIs and recovery of numerous clinical ratings at four consecutive using multi-scale image patches from each MRI using the suggested human brain. The proposed scheme receives 2K image patches from each participant as inputs, and it outputs four different clinical measurements at 4 various time points.

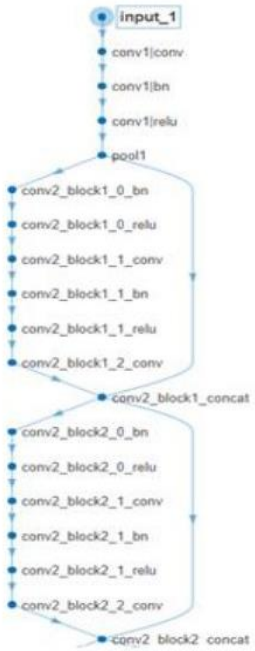

Fig. 2. Proposed Model Network Architecture.

We initially concentrate on modelling the nearby spatial features seen in multi-scale image patchwork using K parallel subnets, each mapped to a particular landmark point. Within every sub-network, the investigators first decrease the effect of the major large-scale update. Therefore, it is a relatively similar diameter to the small-scale patch. These tiny patches are therefore individually sent into a sub-network consisting of three deep convolutional modules (DCMs) and two fully connected (FC) levels, treating them as the two-channel input. In each DCM, three convolutional neural networks are followed by a 222 max-pooling plane for output feature wavelet decomposition. In distinctive, for a precise convolution operation within every DCM, the feature maps (the images that come out of each convolution operation) of all the layers before they are being used as inputs, and the convolution layers of all the layers after they have been used as inputs. Batch standardization and linear transfer unit (ReLU) activation are used after each convolution operation. Such densely linked design strengthens feature propagation, encourages feature reuse, and reduces network parameter optimization. The K parallel subnetworks have identical designs but individually optimized characteristic weights. We want to discover landmark local characteristics from images using K sub-networks to preserve each landmark site's distinctive local analytical information. If sub-networks share properties, we can't extract historic site-local spatial features from brain MRIs.

It is important to note that the overall architecture of an MRI cannot be captured by utilizing merely the local patches alone. To do this, the feature maps knowledge gained since the last K FC layers in K sub-networks are added together, and then two more FC layers are added to learn the neighbourhood classification model of the information MR image. Four clinical-grade categories at four different time points are predicted using the last FC layer (containing 32 neurons). Based on [3], we created a weighted loss function for the network model so that all available loosely labelled training participants could be used to their fullest (missing ground-truth clinical scores). We will refer to the training set of N individuals as $\mathrm{X} = [\mathrm{x}_1, \ldots, \mathrm{x}_\mathrm{n}, \ldots, \mathrm{x}_\mathrm{N}]$, where W refers to the network coefficients. Its sth $(\mathrm{s} = 1, \ldots, \mathrm{S})$ ground-truth clinical value at the $\mathrm{t}-\mathrm{th}$ $(\mathrm{t} = 1, \ldots, \mathrm{T})$ time-point is indicated as $\mathrm{y}_\mathrm{n}^{\mathrm{s,t}}$ for the n^{th} $(\mathrm{n} = 1, \ldots, \mathrm{N})$ subject x_n. The suggested optimization problem aims to reduce the gap here between the following projected number $\mathrm{f}^{\mathrm{s,t}}(\mathrm{x}_\mathrm{n}; \mathrm{W})$ and the actual number $\mathrm{y}_\mathrm{n}^{\mathrm{s,t}}$:

$$arg \min_{W} \frac{1}{N} \sum_{n=1}^{N} \frac{1}{\sum_{t=1}^{T} \sum_{s=1}^{S} \gamma_n^{s,t}} \sum_{t=1}^{T} \gamma_n^{s,t} * \left(y_n^{s,t} - f^{s,t}(x_n; W) \right)^2 \quad (11)$$

Where $\gamma_n^{s,t}$ indicates whether or not x_n is given the s^{th} medical value at the $t-th$ time-point. In particular, if the ground-truth score $y_n^{s,t}$ is accessible for x_n, then $y_n^{s,t} = 0$. To be more particular, even if an instructional subject has omitted scores at some points in time and therefore does not start contributing to the loss of data processing (i.e., $y_n^{s,t} = 0$), it still start contributing to the logistic regression during network training. Therefore, increased throughput is used at various time points. Furthermore, we may have used all accessible individuals (even if they lack ground reality diagnostic ratings at various time intervals) for model training using Eq. (11). It seems possible because (1) allows us to build representations from MR scans informally automatically. The typical beginning of the module dismisses individuals with insufficient ground-truth scores, in contrast to this.

We randomly choose alternative patches centered at each landmark position with separations, and the phase margin is one. This one will increase the training set and lessen the detrimental effect of landmark identification mistakes. As a result, each MRI may also provide 125 patches, one for each point, at each scale. Given K landmarks, we may create 125K variations of patched at each size, each serving as a unique sampling for the neural framework. It technically allows us to create 125K examples for MRI, but these sampling are utilized as input information randomly for the suggested system.

At the training step, designers use the instructional subject matters' BL MRIs as inputs and their own ground-truth diagnostic and therapeutic goals scored at four points in time (with incomplete data) as outputs to train the network. In particular, we firstly collect variations in terms (i.e., 242424 and 484848) image regions from each train MRI and then input such patched to the networks $k-$ Means and k anatomic structures. This method may discover a mapping function from every MRI source to the three clinical ratings at four different periods. During testing step, we first identify its related landmarks using deep learning for an unknown experiment with just a BL MR image and then create a multi-resolution patchwork. We next input these multi-resolution image patches to the trained network to forecast the clinical ratings at four different periods for this test patient.

Stochastic gradient descent (SGD) and the back-propagation technique for generating network concentrations and updating parameters are used to improve the objective function. The mobility parameter and the number of iterations for SGD were explicitly calibrated experimentally to 0.9 and 104. Fig. 3 displays the changing curves for the calibration and testing loss functions on the ADNI-1 database. Using a computer with a solitary GPU, our process utilizes about 12 seconds to forecast the four types of diagnostic tests of the MRI experiment. Inferring the suggested $ws-MTDNN$ approach is anticipated to carry out real-time brain illness diagnosis in practical applications. The software and primarily targeted model are accessible online.

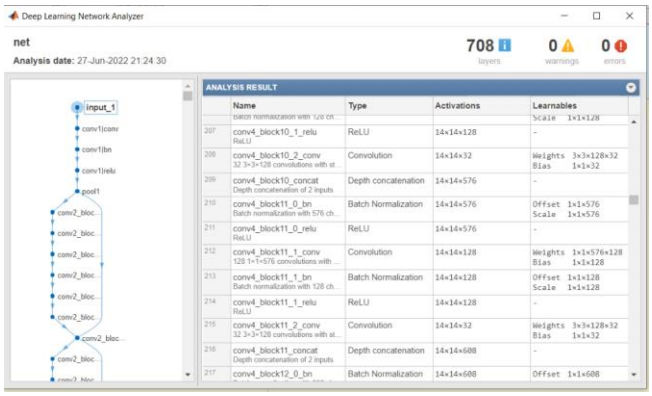

Fig. 3. Layer Description.

V. Numerical Results and Analysis

We execute two sets of trials in twofold confidence intervals to test the suggested method's resilience. We explicitly train models on participants from ADNI-1 and evaluate them from the separate ADNI-2 Dataset in the first set of trials. The second category trains on ADNI-2 and tests on ADNI-1. Various performance metrics like accuracy, specificity, sensitivity and error rate are evaluated and compared with other approaches. The expressions for these metrics are given below:

$$Accuracy = \frac{TP+TN}{TP+FP+TN+FN} \quad (12)$$

$$Sensitivity = \frac{TP}{TP+FN} \quad (13)$$

$$Specificity = \frac{TN}{TN+FP} \quad (14)$$

$$Error\ rate = 1 - \frac{1}{2}(sensitivity + specificity) \quad (15)$$

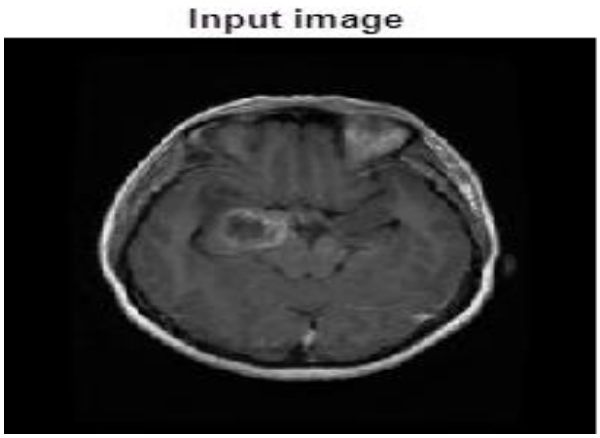

Fig. 4. Input Image.

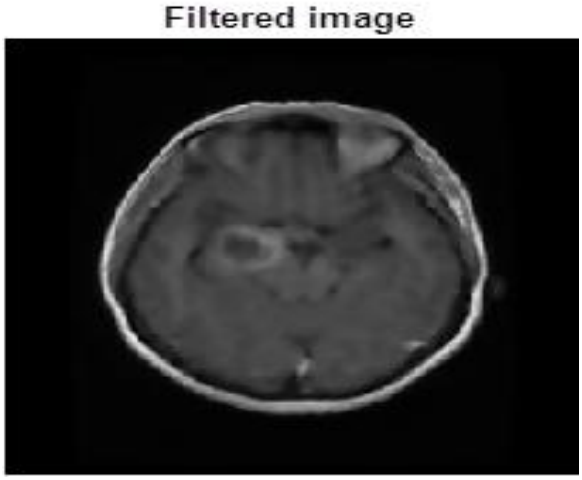

Fig. 5. Filtered Image.

Fig. 4 to Fig. 6 provides the outcome of the pre-processed image. Table 1 compares approaches like conventional ANN, SVM, BoVW-based SVM, conventional CNN and DNN. Here, metrics like accuracy, specificity, sensitivity and error rate are evaluated and compared with other approaches. The accuracy of the anticipated model is 93.08% which is 58.08%, 2.08%, 1.08%, 20.08% and 25.08% higher than other approaches. The specificity of the anticipated model is 83.47% which is 48.47%, 7.47% and 15.47% higher than ANN, conventional CNN and DNN and 6.53% and 9.53% lesser than SVM and BoVW-based SVM model. The specificity of the anticipated model is 100% which is 65%, 9%, 7%, 31% and 35% higher than other methods. The error rate is 0.069 for the anticipated model, which is comparatively lesser than other approaches. Other approaches pose an error rate of 1.2568, 2.564, 3.548, 1.565 and 16.235, respectively. Based on the analysis, it is proven that the anticipated model works well compared to other approaches in the prediction process (See Fig. 7 to Fig. 10).

Fig. 6. Equalized Image.

TABLE I. Overall Comparison

S. No	Methods	Accuracy	Sensitivity	Specificity	Error rate
1	ANN	35	35	35	1.2568
2	SVM	91	90	91	2.564
3	VW-based SVM	92	93	93	3.548
4	Conventional CNN	73	76	69	1.565
5	DNN	68	68	65	16.235
6	WS-MTDNN	93.08	83.47	100	0.069

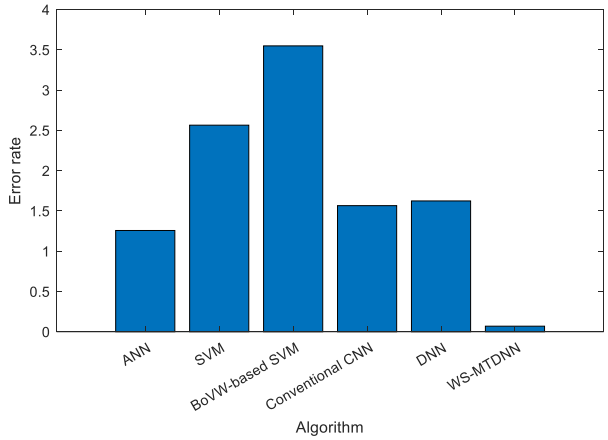

Fig. 7. Error Rate Comparison.

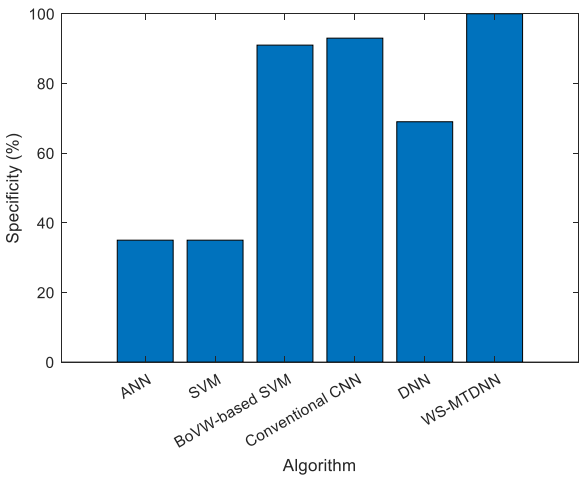

Fig. 8. Specificity Comparison.

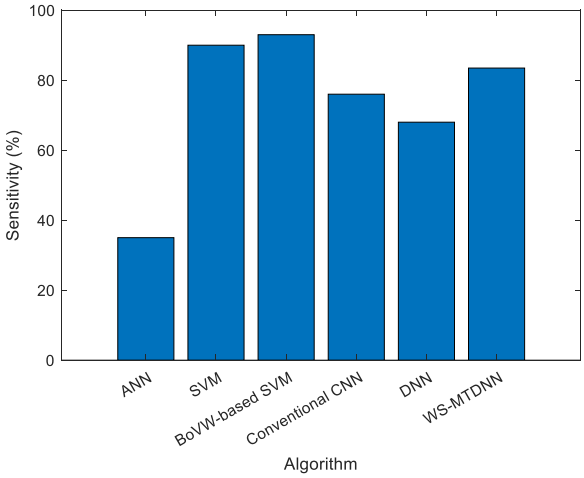

Fig. 9. Sensitivity Comparison.

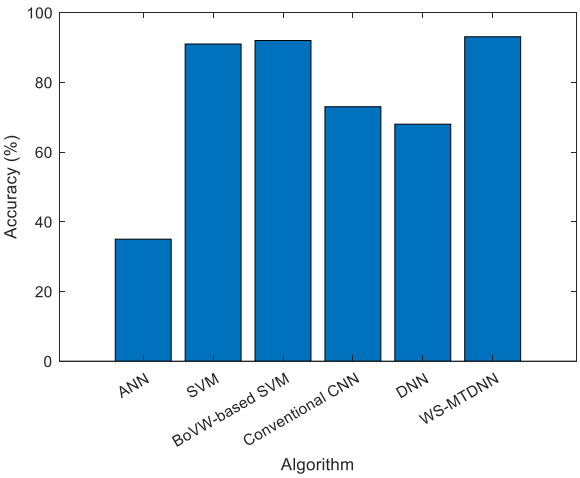

Fig. 10. Accuracy Comparison.

A. Constraint Analysis

The following is a summary of the restrictions this paper still has.

1) The suggested technique was only evaluated for predicting clinical values from MRI images, but ADNI-1 and ADNI-2 databases include transverse MRI scans. The issue with utilizing longitudinally MRI scans for therapeutic score prediction lack subsequent images.

2) The process largely functions for estimating various clinical scores while measuring the relationship among the clinical scores and subject classifications (such as AD or HC).

3) Local patch identification based on anatomic structures is autonomous of extracting the features and classification building, which may hinder prognosis performance.

4) We did not consider the differences in the subject distribution of data between ADNI-1 and ADNI-2. It might adversely impact the generalizability of our technique.

As a result:

1) Users will translational MRI scans to assess the clinical scores. For accurate prediction, missing MRI scans will be filled with learning algorithms (like generative adversarial). Also, full (after calculation) MRI images for evaluating clinical grades at all time points may indicate which time point would be most relevant in disease progression.

2) Given the strong correlation between clinical values and membership functions for a given patient, it seems sensible to create a single deep learning model that combines analysis and categorization.

3) Immediately detect patch/region-level racially discriminatory spots in the entire MRI so patch and region organization contains may be concurrently learnt and merged to build illness classification techniques.

4) We want to develop a better classification approach to address the issue of diverse data distributions. It is anticipated to better the suggested network's capacity to generalize.

VI. Conclusion

In this research, we suggested $ws-MTDNN$ for predicting many clinical scores based on individuals having MRI data and partial clinical ratings. It was done using individuals as training data and individuals as validation data. Specifically, we pre-processed all MR images and then used feature detection algorithms to locate disease-related anatomical structures in the patients' bodies. Based on the position of each landmark, we selected multi-scale patchwork with the landmarks serving as their centres. We constructed a deep convolutional neural network to concurrently learn discriminant information from MRI and forecast several clinical grades at four different periods. The input data for this network were image patches. Our network model constructed a balanced loss function for all training patients, though many may not have full ground-truth clinical ratings. The suggested $ws-MTDNN$ algorithm can identify clinical grades at future time points utilizing MRI data in science experiments from the available datasets.

References

[1] Abiwinanda N, Hanif M, Hesaputra ST, Handayani A, Mengko TR (2019) Brain tumour classification using convolutional neural network.

In: World congress on medical physics and biomedical engineering 2018. Springer, pp 183–189.

[2] Al-Zu'bi S, Hawashin B, Mughaid A, Baker T (2021) Efficient 3d medical image segmentation algorithm over a secured multimedia network. Multimed Tools Appl 80(11):16887–16905.

[3] Ahmed KB, Hall LO, Goldgof DB, Liu R, Gatenby RA (2017) Fine-tuning convolutional deep features for MRI-based brain tumour classification. In: Medical imaging 2017: computer-aided diagnosis, vol 10134. international society for optics and photonics, p 101342e.

[4] Alzu'bi S, Jararweh Y, Al-Zoubi H, Elbes M, Kanan T, Gupta B (2019) Multi-orientation geometric medical volumes segmentation using 3d multi-resolution analysis. Multimed Tools Appl 78(17):24223–24248.

[5] AlZu'bi S, Al-Qatawneh S, Alsmirat M (2018) Transferable hmm trained matrices for accelerating statistical segmentation time. In: 2018 Fifth international conference on social networks analysis, management and security (SNAMS). IEEE, pp 172–176.

[6] Baldi P (2012) Autoencoders, unsupervised learning, and deep architectures. In: Proceedings of ICML Workshop on unsupervised and transfer learning, pp 37–49.

[7] AlZu'bi S, Shehab M, Al-Ayyoub M, Jararweh Y, Gupta B (2020) Parallel implementation for 3d medical volume fuzzy segmentation.

[8] Greenspan, ''Super-resolution in medical imaging,'' Comput. J., vol. 52, no. 1, pp. 43–63, 2008.

[9] Manjón, P. Coupé, A. Buades, V. Fonov, D. L. Collins, and M. Robles, ''Non-local MRI upsampling,'' Med. Image Anal., vol. 14, no. 6, pp. 784–792, Dec. 2010.Manjón, P. Coupé, A. Buades, D. L. Collins, and M. Robles, ''MRI super-resolution using self-similarity and image priors,'' Int. J. Biomed. Imag., vol. 2010, Dec. 2010, Art. No. 425891.

[10] Coupé, J. V. Manjón, M. Chamberland, M. Descoteaux, and B. Hiba, ''Collaborative patch-based super-resolution for diffusionweighted images,'' NeuroImage, vol. 83, pp. 245–261, Dec. 201.

[11] Jafari-Khouzani, ''MRI upsampling using feature-based non-local means approach," IEEE Trans. Med. Imag., vol. 33, no. 10, pp. 1969–1985, Oct. 2014.

[12] Hu, X. Wu, and J. Zhou, ''Second-order regression-based MR image upsampling,'' Comput. Math. Methods Med., vol. 2017, Jan. 2017, Art. No. 6462832.

[13] Buades, B. Coll, and J.-M. Morel, ''A non-local algorithm for image denoising,'' in Proc. IEEE Comput. Soc. Conf. Comput. Vis. Pattern Recognit., vol. 2, Jun. 2005, pp. 60–65.

[14] Takeda, S. Farsiu, and P. Milanfar, ''Deblurring using regularized locally adaptive kernel regression,'' IEEE Trans. Image Process., vol. 17, no. 4, pp. 550–563, Apr. 2008.

[15] Wang, ''Multi-scale image sharpening adaptive to edge profile,'' J. Electron. Imag., vol. 14, no. 1, Jan. 2005, Art. no. 013.

[16] Lopez-Rubio, "Superresolution from a single noisy image by the median filter transform," SIAM J. Imag. Sci., vol. 9, no. 1, pp. 82–115, 2016.

[17] Dong, C. C. Loy, K. He, and X. Tang, ''Image super-resolution using deep convolutional networks,'' IEEE Trans. Pattern Anal. Mach. Intell., vol. 38, no. 2, pp. 295–307, Feb. 2016.

[18] Kim, J. K. Lee, and K. M. Lee, "Accurate image super-resolution using intense convolutional networks," in Proc. CVPR, Jun. 2016, pp. 1646–1654.

[19] Sherubha, "Graph Based Event Measurement for Analyzing Distributed Anomalies in Sensor Networks", Sådhanå(Springer), 45:212, https://doi.org/10.1007/s12046-020-01451-w.

[20] Sherubha, "An Efficient Network Threat Detection and Classification Method using ANP-MVPS Algorithm in Wireless Sensor Networks", International Journal of Innovative Technology and Exploring Engineering (IJITEE), ISSN: 2278-3075, Volume-8 Issue-11, September 2019.

[21] Sherubha, "An Efficient Intrusion Detection and Authentication Mechanism for Detecting Clone Attack in Wireless Sensor Networks", Journal of Advanced Research in Dynamical and Control Systems (JARDCS), Volume 11, issue 5, Pg No. 55-68.

[22] Elbes M, Alzubi S, Kanan T, Al-Fuqaha A, Hawashin B (2019) A survey on particle swarm optimization with an emphasis on engineering and network applications. Evol Intel 12(2):113–129.

[23] Guo X, Yin Y, Dong C, Yang G, Zhou G (2008) On the class imbalance problem. In: 2008 Fourth international conference on natural computation, vol 4. IEEE, pp 192–201.

[24] Gumaei A, Hassan MM, Hassan MR, Alelaiwi A, Fortino G (2019) A hybrid feature extraction method with regularized extreme learning machine for brain tumour classification. IEEE Access 7:36266–36273.

[25] Jain R, Jain N, Aggarwal A, Hemanth DJ (2019) Convolutional neural network-based Alzheimer's disease classification from magnetic resonance brain images. Cogn Syst Res 57:147–159.

[26] Kumar S, Dabas C, Godara S (2017) Classification of brain MRI tumour images: a hybrid approach. Procedia Comput Sci 122:510–517.

[27] Mohan G, Subashini MM (2018) Mri based medical image analysis: Survey on brain tumour grade classification. Biomedical Signal Processing and Control 39:139–161.

[28] Myronenko A (2018) 3d MRI brain tumour segmentation using autoencoder regularization. In: International MICCAI brain lesion workshop. Springer, pp 311–320.

[29] Rizk H, Shokry A, Youssef M (2019) Effectiveness of data augmentation in cellular-based localization using deep learning. arXiv:1906.08171.